

# Attenuation of underwater explosion propagating through porous compressible foam

Kazutaka Kitagawa<sup>\*†</sup>, Tatsuya Nomura<sup>\*\*</sup>, Kiyonobu Ohtani<sup>\*\*\*</sup>, and Atsushi Abe<sup>\*\*\*\*</sup>

<sup>\*</sup>Department of Mechanical Engineering, Aichi Institute of Technology, 1247 Yachigusa, Yakusa, Toyota, Aichi 470-0392, JAPAN  
Phone : +81-565-48-8121

<sup>†</sup>Corresponding author : kitagawa@aitech.ac.jp

<sup>\*\*</sup>Graduate student, Aichi Institute of Technology, 1247 Yachigusa, Yakusa Toyota, Aichi 470-0392 JAPAN

<sup>\*\*\*</sup>Institute of Fluid Science, Tohoku University, 2-1-1 Katahira, Aoba-ku, Sendai, Miyagi 980-0812, JAPAN

<sup>\*\*\*\*</sup>ITOCHU Techno-Solutions Co., Kasumigaseki Bldg., 3-2-5 Kasumigaseki, Chiyoda-ku, Tokyo 100-6080, JAPAN

Received : November 14, 2014 Accepted : June 29, 2015

## Abstract

Collision of underwater explosion and a rigid plate or high porosity foam is investigated experimentally and numerically. As the motivation of this study, it is deduced that attenuation behavior of strong shock environment by porous compressible foam depends on the porosity, cell structure and acoustic impedance in the foam. All foam has open cell type cellular structure, high porosity, low density and low acoustic impedance in comparison with metal and plastic. Experiment on underwater explosion-foam interaction is conducted by using the micro-explosive. Variation of total stress in foam does not show underwater shock pressure-time history and pulsating of the gas bubble. Peak stress of incident shock impingement and bubble pulse in foam with cell number 50 are decreasing up to 99 % and 95 to 98 % of the dynamic pressure value in aluminum plate case. Result of numerical simulation is compared with the experimental findings, which shows essentially same gas bubble motion with experimental result.

**Keywords** : underwater explosion, explosion attenuation, underwater shock wave, environmental problem

## 1. Introduction

Interaction between underwater explosion (UNDEX) and complicated mediums is one of the research topics related to strong impulsive force in structures (oil platform, offshore platform and ship) for disaster prevention from industrial accident explosions<sup>1)–3)</sup>.

The incident shock pressure pulse acts the first injure on a structure due to strong impulsive force and high pressure impingement. The explosive product is produced at high pressure gas region in the liquid by explosion. The collapsing gas bubble motion and bubble jet flow is affected the second injure on whipping the structure by momentum and inertia effect<sup>4)</sup>. Also, the scaled explosion parameters normalized by enables the result of a small scale explosion to convert and to predict into large-scale

one<sup>5),6)</sup>.

Present study is a part of series of research on attenuation and reduction of strong shock environment by porous medias<sup>7)–10)</sup>. Attenuation and reduction effect come from porosity and acoustic impedance in porous materials, and unsteady drag effect for interaction between shock wave passing through three-dimensional complex structure in foam.

The aim of the present research is to investigate the attenuation and reduction effect of underwater explosion by porous elastic material. It is deduced that the dynamic behavior of attenuation and mitigation of underwater explosion corresponds to the inertia and momentum dispersion of incident shock pressure, bubble pulse and bubble jet flow by porous elastic material.

## 2. Experiments

Underwater explosion experiments were conducted by detonating micro-explosive, such as silver azide pellet, and are shown schematically in Figure 1. The silver azide ( $A_g N_3$ ) pellet is delivered as cylindrical charge each with its mass of approximately 10 mg, since the material density is  $3770 \text{ kg m}^{-3}$ , and cylinder with 1.5 mm dia. has aspect ratio (length over diameter) of unity. Micro-explosions could be demonstrated explosive shock loading expected in a full size explosion.

The charge is glued to 1.47 mm core dia. plastic optical fiber (POF) and ignited by the pulsed Nd:YAG laser (532 nm, 5ns pulse duration, 85 mJ per pulse) fed through POF. The pellet is placed at from 30 to 35 mm from the free surface (charge depth) and it horizontally inserted, as shown in Figure 1. Scaled distance  $Z$  were selected from 1.45 to 1.70  $\text{m kg}^{-1/3}$  corresponding the intermediate depth explosion ( $0.40 < Z < 5.55$ ). The face-on overpressure was measured hydraulic shock pressure by piezoelectric Polyvinylidenfluorid (PVDF) needle hydrophone (Müller-Platte-Gauge) at 50 mm (E) from center of charge. The dynamic pressure (gas pressure+hydraulic pressure) profiles in material were conducted by piezo-electric pressure transducers (PCB HM113A21). Pressure transducers were mounted face-on condition on wall (A, B, C and D) as shown in Figure 1. Total stress in foam was measured by same position and same transducers, which were contact with foam skeleton (Foam + gas pressure + hydraulic pressure). Their output includes sum of the contact force of foam skeleton, the gas pressure and the hydraulic pressure inside the foam. The aluminum plate on undersurface was vertically placed on the free surface of tap water, while the foam layer was glued and attached

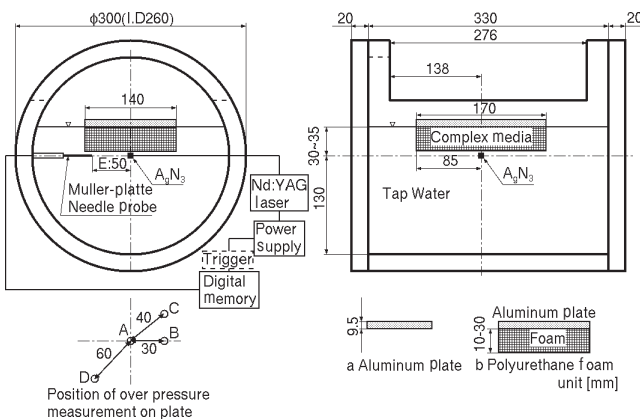


**Figure 1** Schematic description of underwater explosion (UNDEX) experiment.

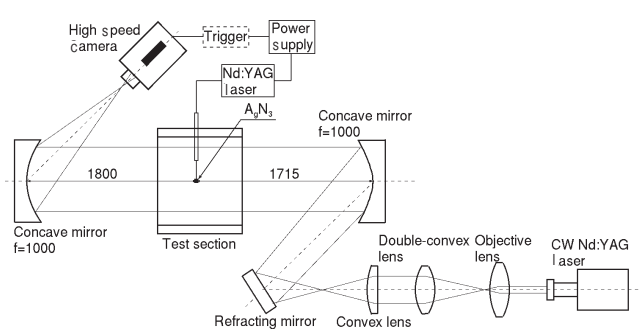


**Figure 2** Optical setup of Shadow graph method.

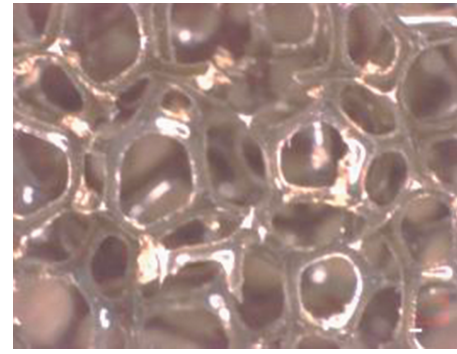


**Figure 3** Cellular structure of open cell type polyurethane foam.

**Table 1** Physical properties of tap water, aluminum and polyurethane foam.

Material	Density $\rho$ [ $\text{kg m}^{-3}$ ]	Sonic speed $c_0$ [ $\text{m s}^{-1}$ ]	Acoustic impedance $10^6$ [ $\text{Pa s m}^{-1}$ ]	Porosity [%]	$x \times y \times z$ [cells $\text{in}^{-1}$ ]	
Tap water	1000	1483	1.48	0	NA	
Aluminum	2680	6420	17.2	0	NA	
Porous material	Foam13	27.5	$\approx 500$	0.0138	97.7	$13 \times 13 \times 13$
	Foam30	31.0	$\approx 500$	0.0155	97.4	$30 \times 30 \times 30$
	Foam50	27.8	$\approx 500$	0.0139	97.7	$50 \times 50 \times 50$

on undersurface of aluminum plate and its other side was free. Time resolved recording of collapsing gas bubble, foam deformation and production of cavitation were visualized by the back light method with a digital high speed camera. The camera was used for Vision Research Phantom V1610; the frame rate was operated at  $10^5$  frame per second. Figure 2 shows optical setup of Shadow graph method. Shadow graph method could be visible intense and strong density change, such as the propagation of shock wave and reflected wave. The high speed camera was used for Shimadzu HPV-2; the frame rate was operated at  $10^6$  frame per seconds.

Characteristics of open cell type polyurethane slab shaped foam, an acrylic and an aluminum are given in Table 1. Figure 3 shows typical cellular structure in foam. The foam has all composed of three dimensional networks of wires. All foams have high-porosity and low-density. Acoustic impedance in foam has existed in differences of 0.008 to 0.009 times comparison with metal material. Three foams with different properties and structures in cell number per unit length, are investigated. In Foam13, cell size and wire diameter of the skeleton network are larger than those of Foam50. The All materials have 140 mm in length, 170 mm in width and 9.5 to 30 mm thickness.

## 3. Numerical simulation

Interaction between underwater explosion and aluminum plate was numerically investigated a multiple solver type hydrocode ANSYS<sup>®</sup> AUTODYN<sup>®</sup>. The multiple material Eulerian solver was used and in which multiple material components: the water, the air and the solid or gaseous phase of the silver azide were included.

The numerical region was the interior of the

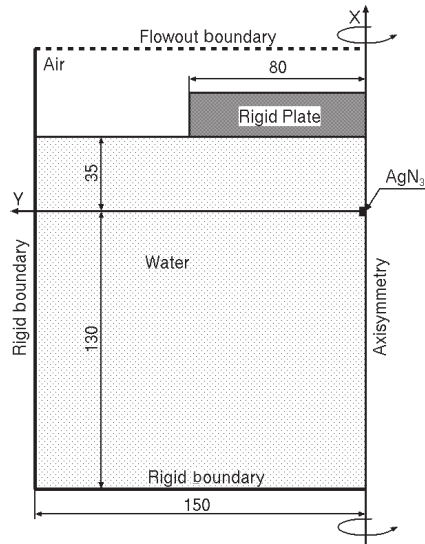


Figure 4 Illustration of numerical model and region.

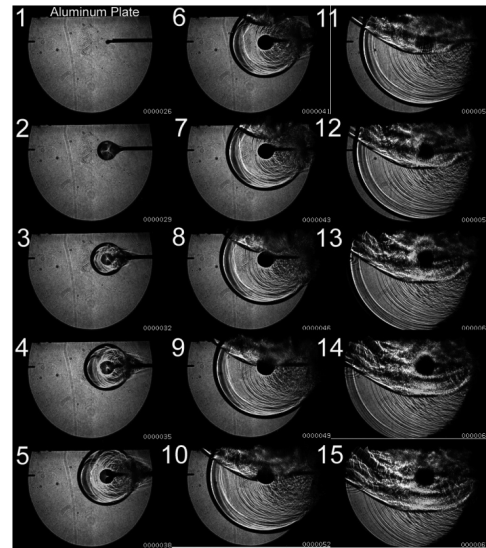
Table 2 JWL parameters for silver azide.

$\rho_0$	$A$	$B$	$R_1$	$R_2$	$\omega$	$D$	$e_0$	$P$
[kg m <sup>-3</sup> ]	[GPa]	[GPa]	[-]	[-]	[-]	[m s <sup>-1</sup> ]	[GJ m <sup>-3</sup> ]	[GPa]
3770	3520	20.6	6.78	1.58	0.193	5480	8.63	22.1

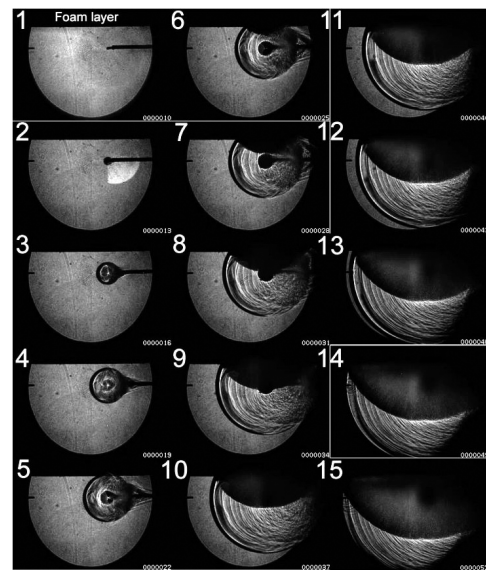
experimental cylindrical acrylic tank with 130 mm inner radius and a two-dimensional axisymmetric numerical model was applied, as shown in Figure 4. The acrylic tank walls were assumed to be rigid. The depth of the liquid, the charge weight of the silver azide, positions of the silver azide and the pressure gauges were numerically set to be identical to the experimental conditions. The air region has a 35 mm height from the liquid surface and a flow-out boundary condition was located on the upper side of the air region. A numerical mesh size was uniformly 0.5 mm in the whole numerical model. Hydrostatic pressure gradient was depending on water depth was given to all over region of water.

Before the calculation by using above numerical model, in order to estimate minutely a detonation phenomenon of a micro silver azide, which conducted a preliminary calculation by using the numerical model only in the vicinity of the explosive with a mesh size of 0.02 mm. The numerical result was transferred to the region-expanded numerical model with a coarser mesh size by using a “remapping” technique in the AUTODYN. Thus, numerical simulation could be simulated sequential phenomena of both the explosion of the micro silver azide and following bubble behaviors.

In water, Mie-Grüneisen type linear shock Hugoniot equation of state (EOS)<sup>11</sup> and spall strength of -3.0 MPa<sup>12</sup> were applied. For tap water, the reference density, Grüneisen parameter  $\Gamma$ ,  $c_0$  and  $s$  denote 1000 kg m<sup>-3</sup>, 0.28, 1483 m s<sup>-1</sup> and 1.75, respectively<sup>13</sup>. Ideal Gas EOS was applied to standard state in air. In silver azide, JWL EOS and programmed ‘on-time burning’ model were applied, and JWL parameters are shown in Table 2<sup>7</sup>. The detonation property of the micro explosive was calculated by using KHT2009.<sup>13</sup>



(a) Aluminum plate



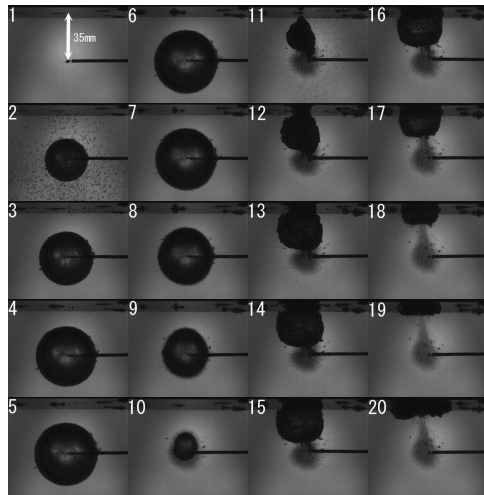
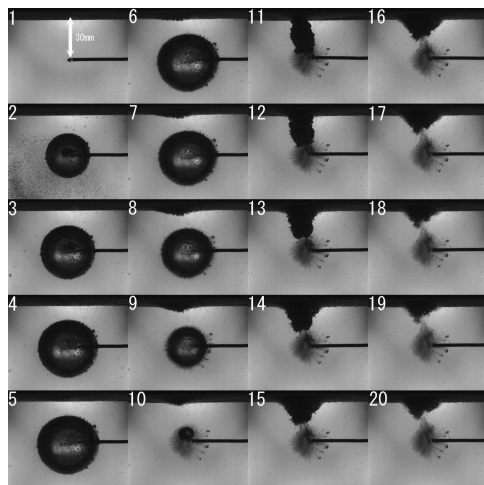
(b) Foam layer (Foam 50)

Figure 5 Sequential Shadow graph image ( $\Delta t = 3 [\mu s]$ ).

#### 4. Results and discussion

Scaled distance  $Z$  of UNDEX experiment were selected from 1.45 to 1.70 m kg<sup>-1/3</sup> corresponding the intermediate depth explosion ( $0.40 < Z < 5.55$ ). The gravity effects on gas bubble motion can be neglected when the ratio of the period of the oscillation cycle of the bubble and a square root of ratio of charge depth and maximum vertical bubble diameter is smaller than 1. The gravity effects can approximately negligible show that the values of the present experiments have within from 0.06 to 0.12.

Figures 5(a) and 5(b) show the sequential Shadow graph image near the aluminum plate and foam layer (Foam 50), respectively. At igniting the explosive, the incident shock wave is traveling spherically and outwardly (frame 1-4). The incident shock wave is reflected on surface as a reflected wave (frame 5-). In aluminum plate, the incident underwater shock wave is propagating and reflecting on surface as compression wave, as shown in Figure 5(a). Propagation of reflected wave on wall surface over takes an underwater shock wave at aluminum plate because sonic speed in aluminum

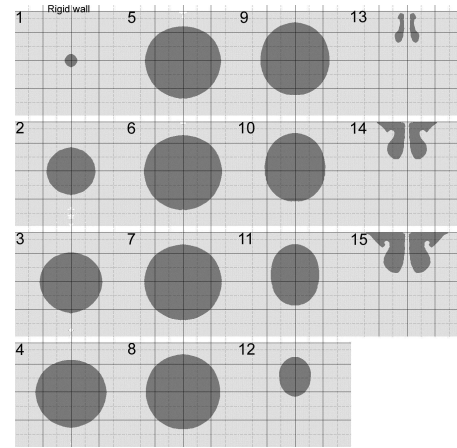
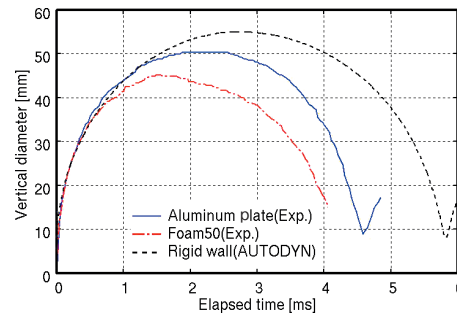
(a) Aluminum plate ( $\Delta t = 0.5$  [ms])(b) Foam layer (Foam50) ( $\Delta t = 0.5$  [ms])**Figure 6** Sequential photographs of the bubble motion.

is higher than water. After frame 7, wave propagation were observed a lot of fringe behind the reflected wave, which correspond to refraction from cutting surface on aluminum plate. In foam layer, the incident shock wave is reflected on foam surface became expansion wave and some shock wave penetrates into the open cell structure, and is shown in Figure. 5(b). Transmitted wave in foam material propagated as compression wave. Gray region (frame 7-) is corresponding the generation of small size of cavitation bubble by reflected expansion wave.

From both Figures 5(a) and 5(b), the velocity of incident shock wave and reflected wave is measured to be about  $1620$  and  $1910 \text{ m s}^{-1}$  in aluminum plate, while it is about  $1700$  and  $1740 \text{ m s}^{-1}$  in foam layer, respectively.

Figures 6(a) and 6(b) show the time resolved transformation of the gas bubble near the aluminum plate and foam layer (Foam50). The gas bubble is growth in expanding phase (Figure 6(a) for frame 1–6 and Figure 6 (b) for frame 1–7). After the maximum size, the pressure inside the gas bubble decreases, and a gas bubble begins in contracting phase (Figure 6(a) at frame 7- and Figure 6 (b) at frame 8-).

In the case of aluminum plate (Figure 6(a)), a gas bubble travels to the wall side and collides with the wall surface by the strong upward water jet flow. It seen from Figure 6

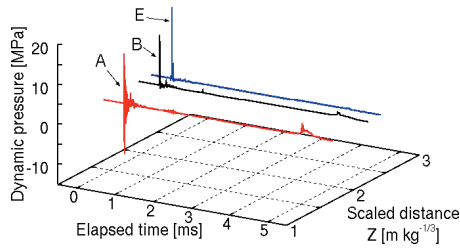
**Figure 7** Numerical results of the bubble motion near the aluminum plate ( $\Delta t = 0.5$  [ms])**Figure 8** Time variations of vertical diameter in gas bubble.

(a), the moving speed on bubble upper side is measured to be about  $44.5 \text{ m s}^{-1}$ . The gas bubble is sticking to a wall surface. Deformation of aluminum plate could not be observed by the intermediate depth UNDEX condition.

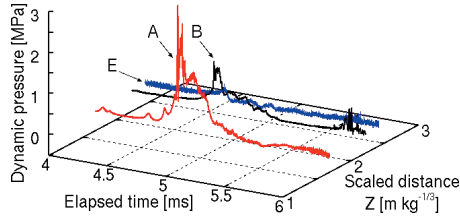
In Figure 6(b) for foam layer, at starting the expansion phase, a gas bubble became ellipsoid shape by effect of moving boundary of foam. The small bubble in foam layer is drawn to the upper side of explosive product. The gas bubble at contraction phase is moving to downward and apart from a foam surface by weak downward flow. Moving velocity of upper side of a gas bubble is evaluated to be about  $27.7 \text{ m s}^{-1}$  in foam layer. Bubble motion decelerated by foam layer.

Figure 7 shows the computed time dependent transformation of the bubble motion in water. The size of square of the solid line is of  $10 \text{ mm}$ . It is seen from Figure 7 that, the computed results simulate the experimental bubble motion well. However, a time difference of  $1.2 \text{ ms}$  has been observed between the experimental and the computational results.

Figure 8 shows time variations of vertical diameter in gas bubble. The bubble reaches maximum size at  $t = 1.4 \text{ ms}$  for foam and  $2 \text{ ms}$  for aluminum plate and kept ellipsoid shape and spherical, respectively. The repeated cycle in Foam 50 is high in about  $0.6 \text{ ms}$  time difference of comparison with the aluminum plate. For Foam 50, after reaching its maximum size, the gas bubble started to collapse and traveled to downward, while for aluminum plate, the water jet is fully developed and going to impact the aluminum plate. It is considered that the incident shock wave penetrates into the foam freely and low acoustic impedance restrains the contraction motion. It is



**Figure 9** Time and space variation of the over pressure under underwater explosion near the acrylic plate.



**Figure 10** Enlargement of time histories of the bubble pulsation under underwater explosion near the acrylic plate.

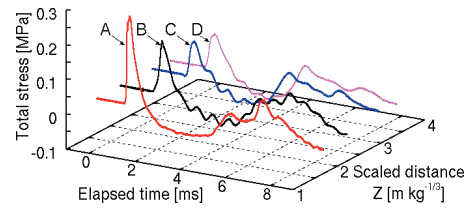
repeated expansion and contraction on wall and also absorbed bubble motion.

Computed result is observed a time difference of 1.2 ms at the repeated cycles in the measured result. As a particular one of several reasons, the numerical model of the silver azide was applied for an ideal state explosion, however the experimental condition is in non-ideal state explosion.

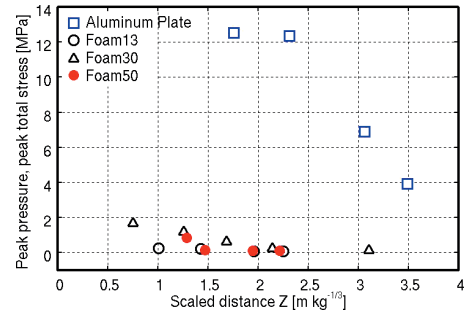
Figure 9 shows typical time variations of experimental dynamic pressure on the aluminum plate (A, B) and hydraulic shock pressure (E). At  $t = 0$  to 0.2 ms on position A, the dynamic pressure variation demonstrated high frequency oscillation, which shows that high frequency oscillation does not indicate exactly the shock impingement phenomena by underwater shock wave. However, the transducer could be measured bubble pulsation. Pressure histories show a first peak pressure by impingement of underwater shock wave, and then pressure decreases quasi-exponentially until the pressure reaches static pressure. At  $t = 4.8$  ms, the second peak pressure show the bubble pulsation.

Figure 10 shows the enlargement of time histories of the bubble pulsation for underwater explosion at position A, B and E. At  $t = 4.8$  ms, it shows the pressure pulses, which are emitted from contraction of a gas bubble closely its minimum. The duration of the bubble pulsations was very long when compared with the pressure-time variation of incident underwater shock wave. The bubble pulsations arise from a much slower than shock wave propagation phenomenon. The bubble pulsations pressure on aluminum plate at A exist difference of up to about 13 times in the bubble pulsations at E.

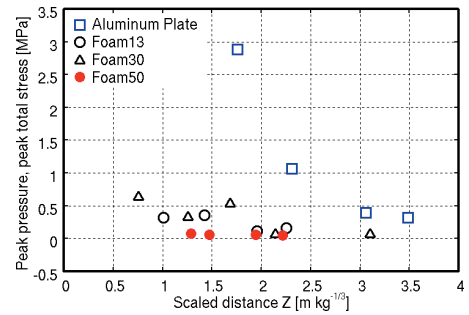
Figure 11 shows typical time variations of total stress in the foam layer (Foam 50). Time oscillation of stresses is increasing very slowly in comparison with the aluminum plate case. Peak stresses and pressure pulse in foam layers decrease much more quickly than that in aluminum plate. Peak stress decreases as distance from the center of the charge increases, due to the momentum loss of



**Figure 11** Time and space variation of the total stress under underwater explosion near the foam with cell number 50 (Foam 50).



(a) First peak value



(b) Bubble pulsation

**Figure 12** Dynamic pressure and total stress versus scaled distance.

underwater explosion by foam layer. It shows that the stress decrease is caused dependent on the cell structure, bubble oscillation cycle and bubble pulsation. Attenuation effect comes from unsteady drag interaction with three-dimensional complex structure in foam.

Figure 12(a) shows the dynamic pressure and total stress at first peak versus scaled distance. Stress attenuation caused in foam with cell number 13 and 50 decreased up to 99 % of the dynamic pressure value in aluminum plate, while the peak stress in foam with cell number 30 decreased from 93 to 94 % in comparison with aluminum plate. Stress attenuation is influenced unsteady drag interaction of incident shock wave with three-dimensional complex structure in foam.

Figure 12(b) shows the dynamic pressure and total stress at bubble pulsation versus scaled distance. Bubble pulsation of the foam with cell number 13, 30 and 50 obtained 85 to 96 %, 80 to 93 %, and 95 to 98 % of the aluminum plate case. The attention effect of total stress in foam is possible to improve from aluminum plate. It indicates that the decrease of total stress is affected the cell structure and cell number.

Figure 13 shows impulse per unit area in bubble pulse as function of the scaled distance. The impulse per unit area is defined as following :

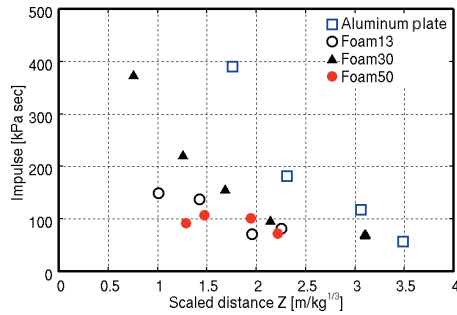


**Figure 13** Impulse per unit area in bubble pulsation versus scaled distance.

$$I = \int_{t_1}^{t_2} p \, dt = \sum_{n=0}^m p_n (t_2 - t_1) = \sum_{n=0}^m \frac{F_n}{A} (t_2 - t_1) [kPa s] \quad (1)$$

Impulse per unit area calculated time limits of integration from positive phase in variation of bubble pulsation pressure. Values  $I$  of the foams decrease as  $Z$  increase.  $I$  of the aluminum plate does not exhibit dispersed and amplified pressure profile in bubble pulsation.  $I$  of the foam with cell number 13, 30 and 50 showed 18 to 44 %, 39 to 60 %, and 26 to 40 % of the aluminum plate case. All foams have about the same density and acoustic impedance, the impulse per unit area became to close value. The foam with cell number 50 has the performance that attenuation effect in pressure impulse has better than other foams.

## 5. Conclusions

Interaction between underwater explosion and porous compressible foam are investigated experimentally and numerically. The motivation of present study is deduced attenuation methods and mitigating condition of underwater explosion by porous foam layers.

Experiments with underwater explosion-compressible foam interaction were conducted by detonating micro-explosive, with paid to attention of impulse and the total stress variation in foam, the dynamic pressure in aluminum plate and visualization of shock wave and gas bubble motion. Underwater explosion generated by micro-explosive near the both materials for  $0.73 < Z < 3$ .

(a) Aluminum plate : The explosive product traveled to the wall side due to bubble jet in the strong upward flow and collided with the wall surface. The incident shock wave propagated spherically and outwardly. Acoustic impedance in an aluminum is higher than waters. shock wave reflected as compression wave and transmitted wave propagated as compression wave in material. The peak dynamic pressure (sum of gas pressure and hydraulic pressure) in bubble pulsation arose up to about 13 times in hydraulic bubble pulsation.

(b) Foam layer : A gas bubble moved in the apart from the wall due to effect of moving boundary of foam layer. The upper part became dented, and a gas bubble deformed in an ellipsoid shape. The incident shock wave reflected on foam surface became expansion wave due to lower acoustic impedance comparison with water. Some shock wave penetrated into the open cell structure. Behind the reflected wave generated the small size of

cavitation bubble from foam material. The foam body is extended by downward bubble jet flow. Total stress (sum of contact stress of foam skeleton, gas pressure and hydraulic pressure) histories in foam showed a stress which is smaller than that due to the aluminum plate case. The duration of stresses showed slowly in comparison with the aluminum plate. Total stress in foam with cell number 13 and 50 attenuated up to 99 % of peak dynamic pressure in aluminum plate. Bubble pulsation of the foam with cell number 50 is highest decrease in pressure among other foam. Attenuation of the stress or pressure was caused dependent on the cell structure and cell number. Impulse per unit area of the all foam layers decreased from 18 to 60 % of the aluminum plate case. Underwater explosion showed the possibility that could attenuate and mitigate by using porous compressible foam.

A numerical simulation was performed for the interaction between underwater explosion and aluminum plate. The multiple material Eulerian solvers were applied for liquid phase, gas phase and the solid or gaseous phase of the micro-explosive. Result of gas bubble motion and geometric shape simulated the experimental finding well. However, the repeated cycle can be seen time difference of 20 % longer by comparing the experimental result.

## Acknowledgement

Part of the work was carried out under the Collaborative Research Project of the Institute of Fluid Science, Tohoku University and Grant-in-Aid for Scientific Research (C) No. 25420134 offered by Japan Society for the Promotion of Science, Japan.

## References

- 1) R.H. Cole, "Underwater explosions", Princeton University press (1948).
- 2) V. Kedrinskii, "Hydrodynamics of Explosion Experiments and Models", Springer (2005).
- 3) B. Le Méhauté and S. Wang, "Water waves generated by underwater explosion", World Scientific (1995).
- 4) K. Ohtani, et al, Proc. 27th Int. Sympo. on Shock Waves, No. 297 (2009).
- 5) C.F. Hung, et al, J. Fluid Mech., 651, 55–80, (2010).
- 6) A.M. Zhang, et al, J. Sound and Vibration, 311, 1196–1212 (2008).
- 7) K. Kitagawa, et al, Sci. and Tech. Energetic Materials, 73, 93–97 (2012).
- 8) K. Kitagawa and A. Abe A, Proc. 7th Int. Sympo. on Scale Modeling (2013).
- 9) K. Kitagawa, et al, Proc. 29th Int. Sympo. on Shock Waves, No. 0246–000156 (2013).
- 10) K. Kitagawa, et al, Int. Conf. on Flow Dynamics (ICFD2014), Sendai, Japan, 82–83 (2014)
- 11) S. P. Marsh (Ed), "LASL Shock Hugoniot Data," SBN 0–520–04008–2, University of California Press, 1980, etc.
- 12) A. Abe, et al, Proc. 15th APS Topical Conf. on Shock Compression of Condensed Matter 1355 (2007).
- 13) K. Tanaka, Sci. and Tech. Energetic Materials, 64, 167–174 (2003).